СООБЩЕНИЯ
ОБЪЕДИНЕННОГО
ИНСТИТУТА
ЯДЕРНЫХ
ИССЛЕДОВАНИЙ
ДУБНА

E7 - 9862

K.-H.Heinig, H.-U.Jäger, H.Richter, H.Woittennek,
W.Frank, P.Gippner, K.-H.Kaun, P.Manfrass

THE SPECTRAL DISTRIBUTION OF INTERMEDIATE L-K MOLECULAR ORBITAL RADIATION IN SYMMETRIC HEAVY ION COLLISIONS

1976

E7 - 9862

K.-H.Heinig, H.-U.Jäger, H.Richter, H.Woittennek*,
W.Frank, P.Gippner, K.-H.Kaun, P.Manfrass

THE SPECTRAL DISTRIBUTION OF INTERMEDIATE L-K MOLECULAR ORBITAL RADIATION IN SYMMETRIC HEAVY ION COLLISIONS

* Zentralinstitut für Kernforschung, Bereich 2, Rossendorf bei Dresden, DDR.

1. INTRODUCTION

Recently non-characteristic x rays emitted in nearly symmetric heavy ion (Z_1)-atom (Z_2) collisions have been studied by some groups. Using impact energies of the order of 1 *MeV* per nucleon and mean-mass solid targets, the Dubna group investigated the high-energy part of the x-ray spectrum which is situated above all characteristic lines. In this energy region there have been found two distinct continua [1,2,3], denoted as C1 and C2. The high-energy part C2 was assumed to be the K molecular orbital (KMO) radiation which is due to radiative decay of $1s\sigma$ vacancies in transiently formed quasimolecules. For the continuum C1 also a quasimolecular origin has been proposed. It has been interpreted [4] to consist mainly of intermediate L–K molecular orbital (ILKMO) radiation caused by $2p\sigma$ vacancies in the quasimolecule. In the framework of this model the energy limits of the continua C1 and the tendencies of the measured yield ratios Y_{C1}/Y_{C2} can be explained [4].

The aim of the present paper is a semi-quantitative investigation of the spontaneous [5] ILKMO and KMO radiation which appears in the spectrum above the characteristic lines. For this purpose we apply (see Chapter 2) the dynamical theory of intermediate molecular phenomena in heavy ion scattering [6]. A similar approach has been employed by Macek and Briggs [7] in their study of KMO radiation in light collision systems. Contrary to the treatment of Macek and Briggs, we take also into account

(i) the possible radiative decay of $2p\sigma$ vacancies immediately after their formation by $2p\sigma-2p\pi$ promotion [8] in "primary" collisions,

(ii) the interference term between the atomic lines and the ILKMO radiation from such primary collisions,

(iii) both the KMO and the ILKMO radiation emitted during secondary collisions between target atoms and a projectile having already a K vacancy.

In Chapter 3 we discuss semi-quantitative correlation diagrams which take into account electron screening. They have been obtained (for symmetric collisions) by scaling H_2^+ diagrams with screened state-dependent nuclear charges. The model is applied in Chapter 4 to Ni – Ni, Ge – Ge and Nb – Nb collisions. For these collision systems which were investigated in recent experiments [1,2,9,10], our non-relativistic description of inner shells and the assumption of $1s\sigma$-vacancy production by a two-step mechanism [11] are reasonable approximations.

2. *THE RADIATIVE DECAY OF $2p\sigma$ VACANCIES PRODUCED BY ELECTRON PROMOTION*

2.1. *Derivation of a Formula for the Spectral Yield*

When ions are moving through a solid, K-shell vacancies can be produced, and one observes both characteristic K series (of isolated ions and target atoms) and quasimolecular x-rays emitted during close collisions of the moving particles with target atoms. A general description of these radiation processes have been given recently by Smith et al. [6]. Expanding the total wave function of the collision problem on stationary atomic or molecular states plus one-photon states and assuming adiabatic motion, they calculated the spectral amplitude of the emitted photons in first order of perturbation theory. If the rotationally induced radiative decay of inner-shell vacancies is further neglected, one obtains (in dipole approximation) the formulae for the spectral yield per vacancy

$$I_i(\omega) = \frac{4e^2\omega}{3c^3\hbar} \sum_f |\vec{D}^c_{fi}(\omega)|^2 \qquad (1)$$

$$\vec{D}^c_{fi}(\omega) = (2\pi)^{-1/2} \int_0^\infty \vec{D}_{fi}(R(t)) \exp[i\omega t - i\int_0^t \bar{\omega}_{fi}(R(t'))dt' - \frac{\Gamma}{2}t]dt \qquad (2)$$

which has been already extensively discussed and applied to $2p\pi-1s\sigma$ electronic transitions by Macek and Briggs [7]. We start from the same formulae, but evaluate them in the framework of our special assumptions on the collision process. First, we consider the collision of a projectile having L vacancies. It is assumed that at the distance of closest approach (at time $t_1 = 0$) with a certain probability one of these L vacancies is transferred to the $2p\sigma$ orbital by $2p\sigma-2p\pi$ electron promotion [8].

After this "primary" collision the $2p\sigma$ vacancy appears with the probability 1/2 as K vacancy in the projectile which is moving through the solid and can form quasimolecules with target atoms in secondary collisions (at times $t = t_j - T_C/2, \ldots, t_j + T_C/2$; $j = 2,3,\ldots,$; T_C is the collision time). In such a way, our initial state $|i\rangle$ having an inner-shell vacancy with total decay rate Γ is time dependent for every close collision. This time-dependence enters the description through the mutual internuclear distance $R = R(t)$ between the ion and its collision partner. The decay of the vacancy state by radiative decay to different final states $|f\rangle$ is described by the transition energy

$$\hbar\bar{\omega}_{fi}(R) = E_i(R) - E_f(R) \qquad (3)$$

and the dipole matrix element

$$\vec{D}_{fi}(t) = \langle f|\vec{v}|i\rangle = -i\bar{\omega}_{fi}(t)\langle f|\vec{r}|i\rangle \qquad (4)$$

which can be expressed by velocity $\vec{v}$ or coordinate $\vec{r}$ of the jumping electron.

Evaluating in analogy to ref. [7] the dipole velocity matrix element $\vec{D}_{fi}(\omega)$ we separate the radiation of the

isolated ion from the MO radiation caused by different close collisions. For this purpose, the deviations of the quantities $\bar{\omega}_{fi}(t)$ and $\vec{D}_{fi}(t)$ from their unperturbed values are introduced

$$\bar{\omega}_{fi}(t) = \omega^{\circ}_{fi} + \Delta\omega_{fi}(t) , \tag{5}$$

$$\vec{D}_{fi}(t) = \vec{D}^{\circ}_{fi} + \Delta\vec{D}_{fi}(t) \tag{6}$$

with $\Delta\omega_{fi} = 0$, $\Delta\vec{D}_{fi} = 0$ for $t \approx (t_j + t_{j+1})/2$ $(j=1,2,\ldots)$.

Now, the integral (2)

$$\vec{D}^{t}_{fi}(\omega) = (2\pi)^{-1/2}\Big[\int_0^{t_2/2}\Delta\vec{D}_{fi}(t)\,B(t)\,dt + \int_0^{t_2/2}\vec{D}^{\circ}_{fi}\,B(t)\,dt + \int_{t_2/2}^{\infty}\vec{D}_{fi}(t)\,B(t)\,dt\Big],$$

$$B(t) = \exp\Big[i(\omega-\omega^{\circ}_{fi})t - i\int_0^t \Delta\omega_{fi}(t')dt' - \frac{\Gamma}{2}t\Big] = e^{i\phi(t)}\;e^{-\frac{\Gamma}{2}t}$$

is divided in some integrals over time intervals including the primary ($2p\sigma$-vacancy-producing) collision or all secondary collisions, respectively.

We integrate the last two terms of this expression by parts and restrict the limits of the remaining integrals on those time intervals T_c in which the integrands differ distinctly from zero. The result is the desired decomposition of the dipole velocity matrix element

$$\vec{D}^{c}_{fi}(\omega) = (2\pi)^{-1/2}\Big[\frac{-\vec{D}^{\circ}_{fi}}{i(\omega-\omega^{\circ}_{fi})-\Gamma/2} + \int_0^{T_c/2}\Big(\Delta\vec{D}_{fi} + \frac{i\vec{D}^{\circ}_{fi}\,\Delta\omega_{fi}}{i(\omega-\omega^{\circ}_{fi})-\Gamma/2}\Big)\times$$

$$\times B(t)dt - \sum_{j=2}^{\infty}\frac{e^{i\phi(t_j)}\;e^{-\frac{\Gamma}{2}t_j}}{i(\omega-\omega^{\circ}_{fi})-\Gamma/2}\int_{-T_c/2}^{T_c/2}\big(\dot{\vec{D}}_{fi} - i\vec{D}_{fi}\Delta\omega_{fi}\big)B(t)dt\Big] \tag{7}$$

into the central line contribution, the MO contribution from the second half of the primary collision and the MO contribution from all secondary collisions. It is provided throughout the present paper that the initial state $|i>$ manifests itself in primary collisions as $2p\sigma$ vacancy and in secondary collisions with equal probabilities either as $1s\sigma$ or as $2p\sigma$ vacancy. During the times between close collisions the projectile has a K vacancy. These specifications will be included in the following formulae by another notation of the indices characterizing the electronic transitions.

Investigating MO radiation which is well separated from characteristic lines, in the evaluation of eq. (7) some further approximations can be made. Evaluating the average of $|\vec{D}^{c}_{fi}(\omega)|^2$ over all path sections of the ion trajectory we assume that the phase factors

$$\exp\Big[i(\omega-\omega^{\circ}_{fi})t_j - i\int_0^{t_j}\Delta\omega_{fi}(t)dt\Big] \qquad (j=2,3,\ldots)$$

average to zero and, thus all path depending cross terms vanish (random phase approximation) /7/. Doing this we neglect also completely the possibility of coherence effects in x-rays from different secondary collisions, which can be caused by periodic structures in the solid target and which have been investigated very recently /12/. The distortion of the central line emission by the secondary collisions (interferences between atomic radiation and MO radiation from secondary collisions) gives raise to the "usual" collision broadening /13/ which appears additionally to the natural line broadening. This is taken into account by an appropriate choice of an effective decay width Γ. Eq. (7) contains, however, no path-depending phase shift between the MO radiation from the vacancy-producing collision and the central line emitted immediately after this collision (up to the next distortion). This may cause coherence effects in the spectrum, too. In order to take into account such effects, we calculate the interference between the first two terms of eq. (7).

Concerning the sum over j in eq. (7) we adopt from ref. /7/ the method to approximate

$$\sum_{j=2}^{\infty} e^{-\Gamma t_j} \approx \frac{v}{\Gamma d},$$

where d is the interatomic separation and v the mean projectile velocity in the target. In our examples this relation is fulfilled with an accuracy of about 10 per cent. The quantity $e^{-\Gamma t/2}$ in the integral over times $-T_c/2 \le t \le T_c/2$ can be replaced by unity. Now, we are able to summarize eqs. (1) and (7) and to average them over impact parameters b between 0 and b_{max}, where b_{max} is of the order of half the mean internuclear separation in the solid. A factor

$$(\pi b_{max}^2 d)^{-1}$$

appears which is just the number density N_0 of atoms per unit volume. Thus our final result for the spectral yield per vacancy is

$$I(\omega) = \frac{4e^2}{3c^3 \hbar 2\pi} \sum_f \frac{1}{(\omega-\omega_{f,k})^2 - \Gamma^2/4} \times$$

$$\times \left\{ \frac{\int_0^{b_{max}} 2\pi b P(b) \left| \vec{D}_{f,k} - i \int_0^{T_c/2} [\vec{D}_{f,k} \Delta\omega_{f,2p\sigma} + (\omega-\omega_{f,k} - \frac{\Gamma}{2i}) \vec{\Delta D}_{f,2p\sigma}] e^{i\phi_{2p\sigma}(t)} dt \right|^2 db}{\int_0^{b_{max}} 2\pi b\, P(b)\, db} + \right.$$

$$+ \frac{N_0 v}{\Gamma} \int_0^{b_{max}} \pi b \Big[\Big| \int_{-T_c/2}^{T_c/2} (\vec{\Delta D}_{f,1s\sigma} - i \vec{D}_{f,1s\sigma} \Delta\omega_{f,1s\sigma}) e^{i\phi_{1s\sigma}(t)} dt \Big|^2 +$$

$$\left. + \Big| \int_{-T_c/2}^{T_c/2} (\vec{\Delta D}_{f,2p\sigma} - i \vec{D}_{f,2p\sigma} \Delta\omega_{f,2p\sigma}) e^{i\phi_{2p\sigma}(t)} dt \Big|^2 \Big] db \right\},$$

$$\phi_i(t) = (\omega-\omega_{f,k})t - \int_0^t \Delta\omega_{fi}(t')dt'. \qquad (8)$$

We introduced in this eq. the function P(b) which is the vacancy transfer probability /14/ to the $2p\sigma$ MO as a result of a collision with impact parameter b. Doing this we assume that the vacancy transfer happens only at distances of closest approach.

The x-ray yield from secondary collisions is weighted in eq. (8) by a factor $N_0 v/\Gamma$ which depends on the target structure and on the free-mean path v/Γ of the ion with an inner-shell vacancy. This dependence gives the possibility /11/ to distinguish in experiment $1s\sigma$-vacancy production by a two-step mechanism from that by direct excitation. In cases where the two-step mechanism dominates, it determines essentially the yield ratio of ILKMO and KMO radiation /4/.

Concerning the derivation of eq. (8) there is one problem which we have not mentioned so far. When a quasimolecule having an inner-shell vacancy is breaking up, the vacancy may remain either in the projectile or in the target atom. If this vacancy transfer to a target atom is accompanied by a neglectably small recoil effect, the vacancy no longer contributes to quasimolecular x-rays from subsequent collisions *. Such a vacancy loss could be taken into account by changing in eq. (7)

$$e^{-\Gamma t_j/2} \longrightarrow \alpha^{(j-1)} e^{-\Gamma t_j/2},$$

where $(1-\alpha)$ is the vacancy transfer probability to the target atom. Consequently one would obtain in eq. (8) a correction

$$\frac{N_0 v}{\Gamma} \longrightarrow \frac{N_0 v}{(1-\alpha)\frac{v}{d} + \alpha\Gamma}$$

which describes the corresponding suppression of the x-ray yield from secondary collisions. Throughout this paper the value $\alpha = 1$ has been used.

---

* In the Doppler shift analysis of KMO x-rays from 200 *MeV* Kr – Zr collisions /15/, quasimolecules with drastically reduced c.m. velocities give no noticeable contribution to the radiation yield.

Table

Constants used in the calculation. The dipole matrix elements D_{fi} and the total decay rates Γ are taken from ref. /16/.

Experiment	$\lvert D\rvert_{2p\pi,1s\sigma}$ (a.u.)	$\lvert D\rvert_{3p\pi,1s\sigma}$ (a.u.)	$\lvert D\rvert_{3d\pi,2p\sigma}$ (a.u.)	$\lvert D\rvert_{4d\pi,2p\sigma}$	Γ (eV/h)	$\frac{\text{Atoms}}{\text{volume}}$ (10^{28} m^{-3})
$^{60}_{28}Ni \rightarrow {}^{28}Ni$	18.6	6.2	9.3	3.1	1.3	9.14
$^{74}_{32}Ge \rightarrow {}^{32}Ge$	21.4	7.4	10.7	3.7	1.8	4.42
$^{93}_{41}Nb \rightarrow {}^{41}Nb$	24.4	10.6	14.1	5.3	4.0	5.56

2.2. Details of the Calculation

According to eq. (8) the spectral yield per vacancy is calculated by integration along the Coulomb trajectories of the nuclei. In order to avoid errors which may come from an un-appropriated use of numerical methods, the integrals have been evaluated independently both by direct integration and by using a fast Fourier transformation. Our assumptions on the dipole matrix element $\vec{D}_{fi}\,R(t))$ and on the vacancy transfer probability P(b) are explained in the following. A method to construct correlation diagrams which provide transition energies $\hbar\bar{\omega}_{fi}\,(R(t))$ of sufficient accuracy is discussed more in detail in Chapter 3. The MO dipole matrix elements $\vec{D}_{f,2p\sigma}\,(R)$ and $\vec{D}_{f,1s\sigma}(R)$ merge in known atomic values in the united- or separated-atom limits, respectively. Guided by a corresponding graphical representation (*fig. 1a*) for singly-ionized atoms, we decided to include in our calculations four electronic transitions which are strong in both atomic limits and to approximate them by constant dipole matrix elements (*fig. 1b, table*). This interpolation is good for the transitions to the $2p\sigma$ MO provided that the quantities $\vec{D}_{fi}(R)$ change smoothly between the atomic limits. Concerning the transitions to the $1s\sigma$ MO the assumption of constant values $\vec{D}_{f,1s\sigma}$ underestimates the high-energetic KMO radiation. The neglect of $2p\sigma - 1s\sigma$ transitions which provide at small internuclear distances up to 50 per cent of the high-energetic KMO radiation acts in the same direction. We tried to compensate these errors to some extent by constant values $\vec{D}_{2p\pi,1s\sigma}$, $\vec{D}_{3p\pi,1s\sigma}$ which are near to the united-atom limit. The total decay rates Γ used are also given in the *table*.

The vacancy transfer probability P(b) to the $2p\sigma$ MO is calculated using the theory as in ref. /14/. The vacancy transfer can be described as resulting mainly from the rotational coupling between the $2p\pi$ and $2p\sigma$ MO at small internuclear distances /18/. In the framework of this two-state approximation one obtaines coupled first-order differential equations

$$\dot{c}_1(t) = \frac{bv}{R^2} f(R)\, e^{i\Phi(t)}\, c_2(t)$$

$$\dot{c}_2(t) = -\frac{bv}{R^2} f(R)\, e^{-i\Phi(t)}\, c_1(t) \qquad (9)$$

$$\Phi(t) = \int_{-\infty}^{t} \bar{\omega}_{21}(t')\,dt',$$

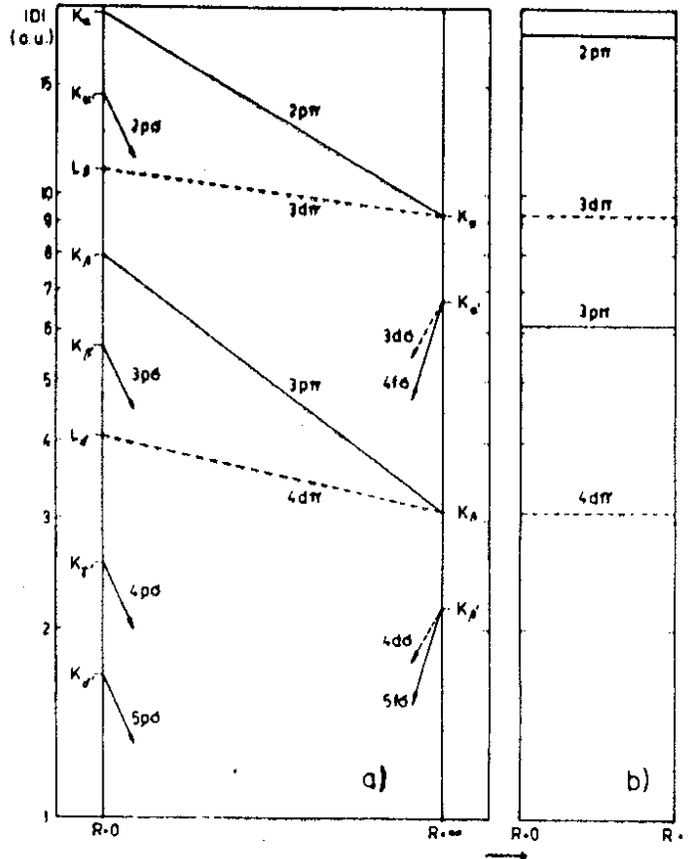

Fig. 1. MO dipole matrix elements $|\vec{D}_{f,1s\sigma}(R)|$ *(solid lines) and* $|D_{f,2p\sigma}(R)|$ *(dashed lines) in the* Ni – Ni *quasimolecule. a) Their schematical behaviour between the atomic radiative transitions calculated in ref.* /16/ *. The notation of the atomic transitions is due to Sommerfeld* /17/*. Arrows indicate that the transition is strongly suppressed in the opposite stomic limit. b) The values used in the present paper.*

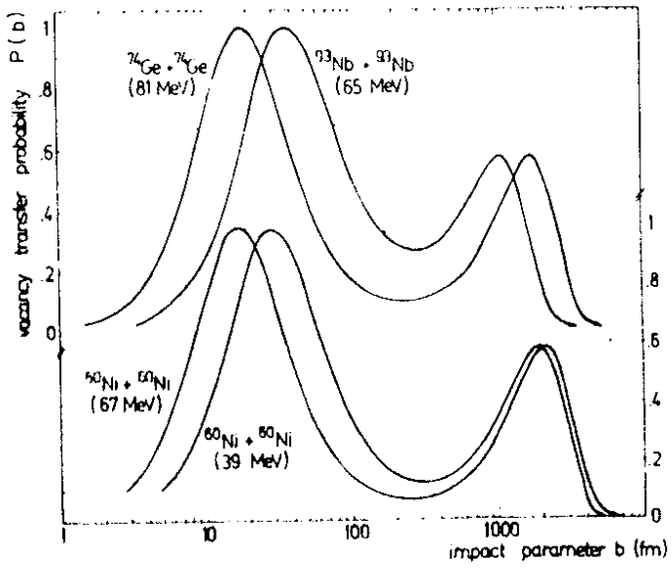

Fig. 2. The vacancy transfer probability P(b) *resulting from rotational coupling between the* $2p\pi$ *and* $2p\sigma$ *MO. The energies given refer to the laboratory system.*

where c_1, c_2 are the amplitude of the $2p\pi$ and $2p\sigma$ MO, respectively. The function f(R) is the rotational coupling matrix element between these orbitals. The initial state is characterized by

$$c_1(-\infty) = 0, \qquad c_2(-\infty) = 1$$

and the total vacancy transfer probability is

$$P(b,v) = |c_1(\infty)|^2. \qquad (10).$$

The solution is rather insensitive to the detailed form of f(R). We use functions f(R) scaled from the $H^+ - H$ problem/19/. Our results for the vacancy transfer probability P(b) in Ni–Ni , Ge–Ge and Nb–Nb collisions are given in *fig. 2.*

3. SEMI-QUANTITATIVE CORRELATION DIAGRAMS

In papers on symmetric ion-atom collisions, H_2^+ correlation diagrams[20] scaled by

$$E = Z^2 E_{H_2^+} \quad , \quad R = R_{H_2^+} / Z$$

have been widely used. Such a one-electron approximation for collision systems with $Z_1 = Z_2 > 1$ neglects electron screening and is reasonable only for the inner shell (and as a guide for qualitative discussions). The $1s\sigma$ MO energy is reproduced with an accuracy of about 25 per cent in the mean-mass region. The relative errors of all other predicted MO energies are very large. Similar arguments hold also for the correlation diagrams of Müller et al.[21] who extended this one-electron description to heavy collision systems by solving the two-center one-particle Dirac equation. Only for a few cases correlation diagrams obtained from Hartree-Fock calculations are available. In the present investigation electronic transitions to the $2p\sigma$ MO play an important role. Therefore, we are interested in correlation diagrams which reproduce with good accuracy the position of the $2p\sigma$ MO and to some extent also those of outer shells. One possibility to obtain such correlation diagrams in a rather simple way opens the variable-screening model of Eichler and Wille[23].

Following an idea of Hund[24], Eichler and Wille split the molecular Thomas-Fermi potential into a sum of two effective (R-dependent) atomic Thomas-Fermi potentials plus a correction term. The effective atomic potentials are chosen in such a way that the correction term is minimized and can be dropped. The remaining effective atomic potentials or their parameters $a_\nu^{eff}(R)$ are known in the separated-atom limit and in the united-atom limit. Between these two limits the quantities $a_\nu^{eff}(R)$ are interpolated by generalizing Hund's interpolation prescription

$$a_\nu^{eff}(R) = \frac{a_\nu^{eff}(\infty)\lambda^2 (\frac{R}{2})^2 + a_\nu^{eff}(0) r_\nu^2}{\lambda^2 (\frac{R}{2})^2 + r_\nu^2}, \quad (\nu = 1,2). \qquad (11)$$

Here, the index ν characterizes the atomic constituents considered. The quantities r_ν are the radial electronic coordinates relative to the nucleus ν. According to general arguments the new parameter λ should be about two. Eichler and Wille found that $\lambda^2 = 3.5$ is an optimum value for the homonuclear molecules $N_2, \ldots, Ar_2$. Within the region $\lambda^2 = 3, \ldots, 4$ the results depend weakly on this parameter.

Applying formula (11) one obtains effective "atomic" quantities depending on the internuclear distance R and on the electronic coordinates. This approach must be considered as a pure phenomenological one since there is no derivation of this interpolation prescription. Aside from a certain arbitrariness in the choice of the functional form of eq. (11), there is also some ambiguity in its application. The use of this method is justified in the main by the large success of Hund[24] and Eichler and Wille[23] in calculating molecular quantities.

Our aim is to introduce with the help of eq. (11) screened effective charges

$$Z_\nu^{eff}(R) = \frac{Z_\nu^{eff}(\infty)\lambda^2 (\frac{R}{2})^2 + Z_\nu^{eff}(0) r_\nu^2}{\lambda^2 (\frac{R}{2})^2 + r_\nu^2}. \qquad (12)$$

In the limiting cases the charges of the two effective atomic Thomas-Fermi potentials can be replaced by the orbital-dependent quantities of the atomic model of Slater

$$\begin{aligned} Z_1^{eff}(R=\infty) = Z_2^{eff}(R=\infty) &\longrightarrow Z_{n\ell}^{ua}, \\ Z_1^{eff}(R=0) + Z_2^{eff}(R=0) &\longrightarrow Z_{n'\ell'}^{ua}. \end{aligned} \qquad (13)$$

Let us further replace the coordinates r_ν in eq. (12) by mean values $\langle r_\nu \rangle$ which depend in a simple way also on the limiting cases $|n\ell\rangle$, $|n'\ell'\rangle$ and change only up to internuclear distances $R_{n\ell n'\ell'}$ where the corresponding atomic orbitals (in dependence on their orientation) begin to separate

$$\langle r_\nu \rangle = \begin{cases} \langle n\ell|r|n\ell\rangle & \text{for } R \geq R_{n\ell n'\ell'} \\ \langle n'\ell'|r|n'\ell'\rangle + \dfrac{R}{R_{n\ell n'\ell'}}\left[\langle n\ell|r|n\ell\rangle - \langle n'\ell'|r|n'\ell'\rangle\right] & \text{for } R \leq R_{n\ell n'\ell'}. \end{cases} \quad (14)$$

Summarizing formulae (12)-(14) it is possible to define also for molecules screened charges which depend on the molecular orbital i and its asymptotic atomic states and which are the same for both centers

$$Z_i^{eff}(R) = \frac{Z_{n\ell}^{us}\lambda^2(\frac{R}{2})^2 + Z_{n'\ell'}^{us}\langle r_i\rangle^2/2}{\lambda^2(\frac{R}{2})^2 + \langle r_i\rangle^2}. \quad (15)$$

These new effective charges can be used to take into account electron screening approximately in a H_2^+-like description of homonuclear diatomic molecules

$$E_i(R) \approx [Z_i^{eff}(R)]^2 \cdot E_{i,H_2^+}(R \cdot Z_i^{eff}(R)). \quad (16)$$

All data entering into formulae (14)-(16) are available. Using the H_2^+ correlation diagram /20/ and the Hartree-Fock results of Froese Fischer /25/ we constructed correlation diagrams for the (neutral) collision systems Ne–Ne (*fig. 3*), Ni–Ni (see also *fig. 3*), Ge–Ge and Nb–Nb. The Ne–Ne diagram obtained in such a simple way is compared in *fig. 3* with the corresponding results of Eichler and Wille /23/.

Concerning the $2p\sigma$ and $1s\sigma$ shells which are here of special interest, the deviations in *fig. 3* range up to about 15 per cent. These deviations are only to some extent actual errors of our approach, since (contrary to the calculation performed in ref. /23/) the atomic limits are exactly reproduced in our cases. Going to the heavier systems investigated in the present paper, the effect of electron screening on inner-shell positions decreases

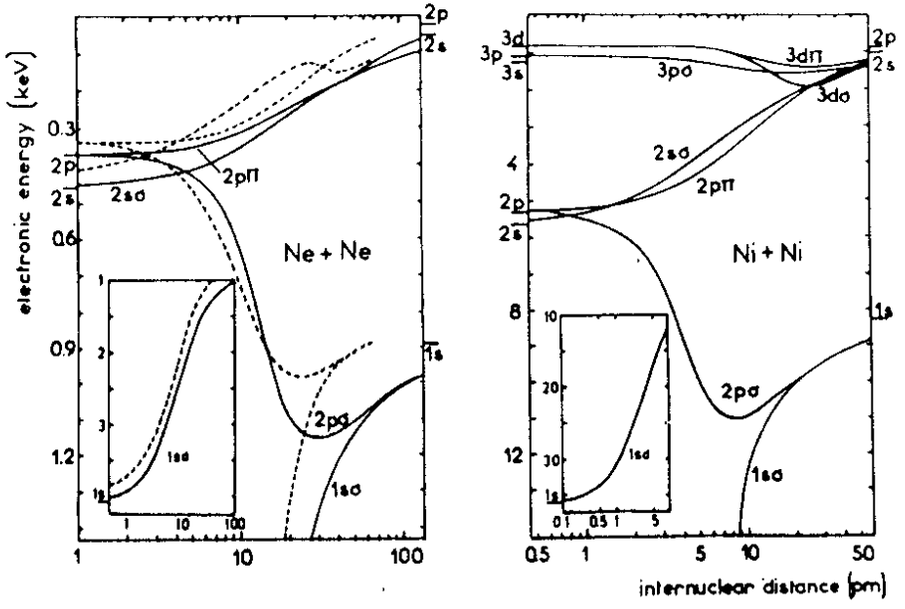

Fig. 3. Ne–Ne *and* Ni–Ni *correlation diagrams obtained by scaling the* H_2^+ *-diagrams* /19/ *with state-dependent screened nuclear charges. For comparison the dashed lines represent the* Ne–Ne *diagram of Eichler and Wille* /22/

in comparison with nuclear attraction. Thus, we expect that our semi-quantitative correlation diagrams provide transition energies $\hbar\bar{\omega}_{fi}$ of an accuracy which is sufficient for our purposes. Relativistic effects are neglected in our correlation diagrams. The corresponding errors of the single-particle energies are in extreme cases (Nb–Nb , united -atom limit) less than 20 per cent, as it can be estimated by comparing the results of non-relativistic Hartree-Fock calculations with those of relativistic Dirac-Fock calculations /26/ for the united-atom limit.

4. DISCUSSION OF THE RESULTS

The aim of the present paper is to describe the gross structure of high-energy non-characteristic x-ray spectra emitted in symmetric ion-atom collisions. Therefore, we restrict ourselves on the investigation of the creation and the spontaneous radiative decay of a K-shell vacancy in an ion moving through the solid. Other effects as, for example, induced radiative transitions /5/ which are much more visible in the anisotropy than in single spectra have not been taken into consideration. In the derivation of our formulae discussed in detail in the preceding chapters, a series of further approximations ("sudden" $2p\sigma - 2p\pi$ electron promotion with probability $P(b)$ at time $t \approx 0$, no vacancy transfer to target atoms, constant dipole matrix elements, semi-quantitative non-relativistic correlation diagrams) had to be made which altogether are expected to give rise possibly to errors of a factor 2. In this connection it is also worth-while to mention that the dependence of the results on the degree of ionization of the ion has been completely neglected. All parameters which have been adopted from the two atomic limits refer to neutral or singly-ionized systems. Especially, fluorescence yields of singly-ionized atoms have been used to estimate the total (Auger- and spontaneous radiative transitions) decay rate Γ (*table 1*).

The photon yields per vacancy $I(\omega)$ calculated according to eq. (8) cannot be compared in a straighforward way with data obtained from experiment. Because of the lack of detailed knowledge on the charge states of the ions and the corresponding K-shell fluorescence yields, the measurements provide only the yield of non-characteristic photons per photon in the characteristic lines. Consequently, we can compare in *figs. 4* and *5* only theoretical and experimental quantities which differ from each other by unknown factors which are of the order of unity. In *fig. 4*, this comparison is made with data from a Ni + 39 *MeV* ^{60}Ni experiment. In this measurement a thin target (85 $\mu g/cm^2$) of natural Ni has been used. The spectrum obtained was corrected for

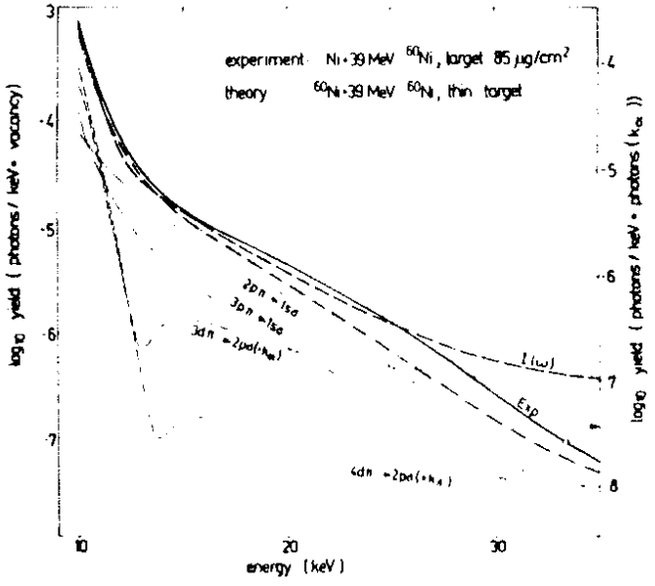

Fig. 4. Comparison of experimental (solid line) and theoretical (dashed line) photon yields in Ni + *39 MeV* ^{60}Ni *collisions. The measurements were carried out with a thin target (85µg/cm²) placed at an angle of 45° with respect to the beam direction, whereas the x-ray emission was measured at 90°. The spectrum given is corrected for detector efficiency. The delayed background as well as electronic and nuclear bremsstrahlung /27/ have been subtracted. Concerning the theoretical results, there are given separately the contributions of the radiative transitions having been taken into account. The dashed-dotted curve has been obtained by omitting the central line contribution.*

detector efficiency. The delayed background, electronic and nuclear bremsstrahlung /27/ have been subtracted. Generally, the experimental data of MO radiation were taken using additional absorbers to suppress the intensities of the characteristic lines and to avoid pile-up contributions to the non-characteristic spectra. This leads to a considerable descending of the detector efficiency curve even in this energy region where the characteristic lines arise. In order to reduce the experimental errors

we obtained the $K_{\alpha,\beta}$ yields usually in a second measurement, where besides of the reaction chamber wall and the Be window of the detector no additional absorbers were used. But, in our Ni + 39 *MeV* ^{60}Ni and Ge+81 *MeV* ^{74}Ge spectra we used for experimental reasons the $K\beta/K_\alpha$ intensity ratios of ref.[29] obtained for electron bombardment. The corresponding experimental results given in *figs. 4* and *5b* may therefore be overestimated.

In ref.[4] we discussed x-ray spectra which were not corrected for detector efficiency. In such spectra a two-component structure of the high-energy Ni–Ni MO continuum cannot be seen. However, if one considers Ni–Ni spectra corrected for detector efficiency (*figs, 4* and *5*), two distinct continua C1 and C2 also appear. At incident energies as 39 *MeV*, K-shell excitation by rotational coupling of the $2p\sigma$ and $2p\pi$ orbitals with an L-shell vacancy dominates[28], and the formalism developed in Chapter 2 can be applied. Thus, the Ni–Ni spectrum of *fig. 4* is a suitable example to check quantitatively our suggestions[4] on the superposition of ILKMO and KMO radiation. We present in *fig. 4* the theoretical yield per vacancy $I(\omega)$ and also the contributions of strong radiative MO transitions to this quantity calculated according to eq. (8). Since we take into consideration the interference between central lines and the ILKMO radiation from primary collisions, there can be presented only the sum of ILKMO radiation and central line wings. At photon energies $E_x = 10,\ldots, 25$ *keV*, we obtain a spectral distribution $I(\omega)$ which is very similar to the measured one. Concerning the normalization, the experimental and theoretical curves in *fig. 4* differ by a factor 3 which is understandable because of the uncertainties in this comparison discussed already above. We think that the achieved agreement strongly supports both the suggestions[4] on the appearance of KMO and ILKMO radiation in the spectrum and the assumptions on the reaction mechanism adopted in this investigation.

In *fig. 4*, the ILKMO radiation ranges in practice only up to about $E_x = 15$ *keV*. Above these energies the two corresponding curves consist of pure K_α and K_β line

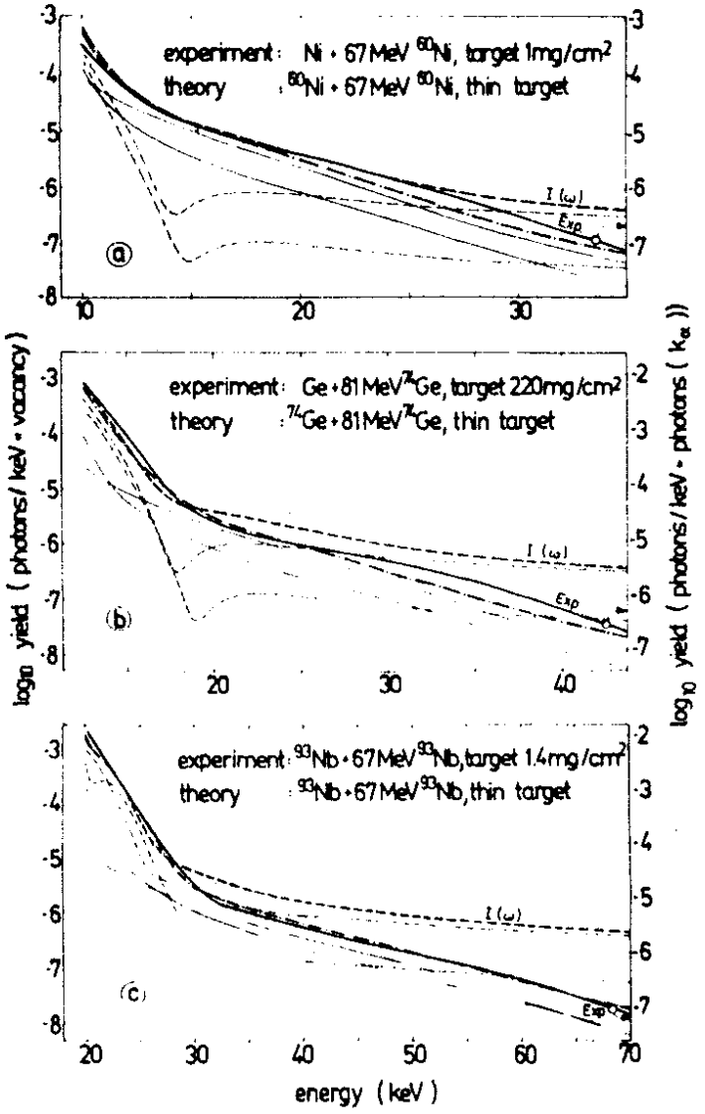

Fig. 5. Qualitative comparison of thick-target measurements and theoretical spectral yields per vacancy for Ni–Ni , Ge–Ge *and* Nb–Nb *collisions; for further details, see fig. 4.*

tails, respectively. Especially, above $E_x \approx 25$ *keV* the K_α line tail begins to exceed all MO contributions. The deviations of $I(\omega)$ from experiment which arise in the same energy region seem to be closely related to this dominance of the K_α line tail. If the atom line contribution (first term in eq. (7)) is omitted formally in the calculation of the spectrum (dashed-dotted line in *figs 4* and *5*), one obtaines at high frequencies an essentially better agreement with experiment. This result suggests to think about line profiles at frequencies far from the line center (here $\omega \gtrsim 4\omega_0$, $\Gamma \ll \omega_0$). In the general consideration (see e.g., ref. /30/) leading to a Breit-Wigner distribution

$$I(\omega) \sim \frac{\omega}{(\omega-\omega_0)^2+\Gamma^2/4}$$

it is provided in the framework of a two-state approximation that the decay of the excited state at time $t=0$ suddenly begins. The validity of these initial conditions in our cases requires a more careful investigation. Using the uncertainty relation $\Delta E \cdot \Delta t \approx \hbar$ one can see that the emission of photons with energies $h\omega \approx \hbar\omega_0 + \Delta E$ far ($\Delta E \approx 20$ *keV*) from the transition energy $\hbar\omega_0$ depends on perturbed initial conditions during a short time interval of the order

$$\Delta t \approx \hbar/\Delta E \approx 10^{-19}\,s.$$

These are just times which characterize the vacancy production by electron promotion according to eqs. (9). Thus, the deviations from experiment at high frequencies should be due to the separate treatment of vacancy production and vacancy decay. This effect will be discussed in more detail in a forthcoming paper.

For the collision systems Ni + 67 *MeV* Ni, Ge + 81 *MeV* Ge and Nb + 67 *MeV* Nb, we can compare the calculated spectrum $I(\omega)$ only with data from thick-target measurements (*fig. 5*). Such a comparison is still meaningful since the radiation yield per vacancy $I(\omega)$ weakly depends on the impact energy (compare *figs. 4* and *5a*, see also the simple estimation in ref. /4/), i.e., a correction of $I(\omega)$ for thick-target effects would require in the main to take into account the energy-dependent x-ray absorption in the target. Apart from this problem, the pre-assumption of an adiabatic and non-relativistic description become in these cases a bit more questionable. Nevertheless, the comparison made in *fig. 5* reveals completely the same kind of agreement between theory and experiment as has been discussed above already for the Ni + 39 *MeV* Ni system.

The dipole velocity matrix element $D^c_{fi}(\omega)$ contains the addition of all radiation along the ion path. If from two or more points of the trajectory the same frequencies are emitted, the interference between them may cause an oscillatory spectrum. This has been noted by several authors /5,7,31/. Especially, there has been discussed the possibility of interferences

(i) between incoming and outgoing ion trajectories /7,32/
(ii) between radiation from subsequent collisions /12/ and
(iii) an oscillating structure which reflects sudden rearrangements of orbital populations in the intermediate molecular systems /32/.

We mention here that ILKMO radiation from the outgoing ion trajectories in primary collisions alone may also interfere because of the minimum in the $2p\sigma$ MO energy. The last effect and the interferences between incoming and outgoing ion trajectories in a given collision have been correctly taken into account in our evaluation of the spectral distribution. We obtain, however, smooth curves which nicely agree with data from a thin-target experiment. A more detailed analysis shows that in our examples the interference pattern in the KMO radiation is obscured by the contributions from different impact parameters, whereas the absence of structures in the ILKMO spectra from primary collisions is due to Heisenberg broadening. Realizing an experiment with a selection of impact parameters an oscillating structure in the C2 continuum should be observed.

5. CONCLUSIONS

An investigation of spontaneous ILKMO and KMO radiation from symmetric collisions in the framework of the dynamical theory provides spectra whose shape and normalization agree with experiment. The calculations reproduce the two-component structure [1-4] of high-energy x-ray continua in collisions between mean-mass systems. Because of average over impact parameters in these experiments the spectra considered have no further structures. These results can be obtained using H_2^+ correlation diagrams scaled by state-dependent effective charges. In the KMO region central line tails must not accepted from a Breit-Wigner distribution. The investigation of line profiles in this region which is far from the line center requires to include the special kind of excitation of the radiating state.

The authors wisth to express their gratitude to Academician G.N.Flerov for his interest in and support of the work. We would like to thank also Dr. L.Münchow for valuable discussions.

References

1. P.Gippner, K.-H.Kaun, F.Stary, W.Schulze and Yu.P.Tretyakov. JINR, E7-7636, Dubna, 1973; Nucl. Phys., A230, 509 /1974/.
2. P.Gippner, K.-H.Kaun, H.Sodan, F.Stary, W.Schulze and Yu.P.Tretyakov. Phys. Lett., 52B, 183 /1974/; W.Frank, P.Gippner, K.-H.Kaun, H.Sodan, W.Schulze and Yu.P.Tretyakov. JINR, E7-8616, Dubna, 1975.
3. W.Frank, P.Gippner, K.-H.Kaun, H.Sodan and Yu.P.Tretyakov. Phys.Lett., 59B, 41 /1975/.
4. K.-H.Heinig, H.-U.Jäger, H.Richter and H.Woittennek. Phys.Lett., 60B, 249 /1976/.
5. B.Müller, R.Kent Smith and W.Greiner. Phys. Lett., 49B, 219 /1974/; B.Müller and W.Greiner. Phys. Rev. Lett., 33, 469 /1974/.
6. K.Smith, B.Müller and W.Greiner. J.Phys., B8, 75 /1975/.
7. J.-H.Macek and J.-S.Briggs. J.Phys., B7, 1312/1974/
8. W.Lichten. Phys. Rev., 164, 131 /1967/.
9. J.S.Greenberg, C.K.Davis and P.Vincent. Phys. Rev. Lett., 33, 473 /1974/.
10. W.Frank, P.Gippner, K.-H.Kaun, P.Manfrass and Yu.P.Tretyakov. JINR, E7-9065, Dubna, 1975.
11. W.E.Meyerhof, T.K.Saylor, S.M.Lazarus, A.Little, B.B.Triplett, L.F.Chase Jr. and R.Anholt. Phys. Rev.Lett., 32, 1279 /1974/.
12. M.Gros and W.Greiner. Z.Physik/, A274, 165 /1975/.
13. V.Weisskopf. Z.Physik., 75, 287 /1932/; Phys. Zeit. 34, 1 /1933/.
14. J.S.Briggs and J.H.Macek. J.Phys., B5, 579 /1972/; J.H.Macek and J.S.Briggs. J.Phys., B6, 842 /1973/; G.Astner, J.D.Garcia and L.Liljeby. J.Phys., B8, L314 /1975/.
15. W.E.Meyerhof, T.K.Saylor and R.Anholt. Phys. Rev., A12, 2641 /1975/.
16. J.H.Scofield. Phys. Rev., 179, 9 /1969/; W.Bambynek, B.Crasemann, R.W.Fink, H.-U.Freund, H.Mark, C.D.Swift, R.E.Price, P.Venugopala Pao, Rev. Mod. Phys., 44, 716 /1972/.
17. A.Sommerfeld. Atombau und Spektrallinien, Vieweg, Braunschweig, 1950, p. 262.
18. J.S.Briggs and K.Taulbjerg. J.Phys., B8, 1909 /1975/.
19. D.R.Bates and D.Sprevak. J.Phys., B4, L47 /1971/.
20. D.R.Bates and R.H.G.Reid. Adv. At. Mol. Phys., 4, 13 /1968/.
21. B.Müller and W.Greiner. Z.Naturforsch., 31A, 1 /1976/; B.Müller, J.Rafelski and W.Greiner. Phys. Lett., 47B, 5 /1973/.
22. F.P.Larkins. J.Phys., B5, 57 /1972/; J.S.Briggs and M.R.Hayns. J.Phys., B6, 514 /1973/; B.Fricke, K.Rashid, P.Bertoncini and A.C.Wahl. Phys. Rev.Lett., 34, 243 /1975/.
23. J.Eichler and U.Wille. Phys. Rev.Lett., 33, 56 /1974/; Phys. Rev., A11, 1973 /1975/.
24. F.Hund. Z.Phys., 77, 12 /1932/.
25. C.Froese Fischer. Atomic Data, 4, 301 /1972/; Atomic Data and Nucl. Data Tables, 12, 87 /1973/.
26. J.P.Desclaux. Atomic Data and Nucl. Data Tables, 12, 312 /1973/.
27. P.Gippner. JINR, E7-8843, Dubna, 1975.
28. R.Laubert, H.Haselton, J.R.Mowat, R.S.Peterson and I.A.Sellin. Phys. Rev., A11, 135 /1975/.
29. G.C.Nelson, B.G.Saunders and S.I.Salem. Atomic Data, 1, 377 /1970/.

30. *W.H.Louisell. Radiation and Noise in Quantum Electronics, McGraw-Hill, New York, 1964.*
31. *W.Lichten. Phys.Rev., A9, 1458 /1974/.*
32. *R.Kent Smith, B.Müller, W.Greiner, J.S.Greenberg and C.K.Davis. Phys. Rev.Lett., 34, 117 /1975/.*

Received by Publishing Department on June 6, 1976.